Available online at www.sciencedirect.com
SCIENCE DIRECT®
International Journal of Heat and Mass Transfer 49 (2006) 2446–2457
International Journal of HEAT and MASS TRANSFER
www.elsevier.com/locate/ijhmt

Prediction of two-phase pressure drop and void fraction in microchannels using probabilistic flow regime mapping

E.W. Jassim *, T.A. Newell

Department of Mechanical and Industrial Engineering, University of Illinois at Urbana-Champaign, 1206 West Green Street, Urbana, IL 61801, USA

Received 8 June 2005; received in revised form 26 September 2005
Available online 11 April 2006

Abstract

Probabilistic two-phase flow map pressure drop and void fraction models are developed for 6-port microchannels in order to provide a more accurate and common means of predicting void fraction and pressure drop. The models are developed for R134a, R410A, and air–water in 6-port microchannels at 10 °C saturation temperatures, qualities from 0 to 1, and mass fluxes varying from 50 to 300 kg/m^2 s. The probabilistic flow map models developed are found to accurately predict void fraction and pressure drop for the entire quality range and for all three fluids.

Keywords: Two-phase flow; Microchannels; Pressure drop; Void fraction; Probabilistic mapping

1. Introduction

Numerous two-phase pressure drop and void fraction models have been developed for microchannels. Each model is developed using assumptions of the physics of the flow, which are accurate for a specific flow regime. However, models that accurately predict pressure drop and void fraction for all flow regimes without discontinuities could not be found in the literature.

In this paper new probabilistic two-phase flow map models are developed in order to predict pressure drop and void fraction for a wide range of qualities and mass fluxes where different flow regimes exist. Curve fits were made for flow regime time fractions for R410A, R134a, and air–water at mass fluxes of 50, 100, 200, and 300 kg/m^2 s for qualities from 0 to 1 in the liquid, intermittent, vapor, and annular flow regimes. Pressure drop and void fraction models for each flow regime were chosen for incorporation into the microchannel models. The method is general, however, such that other flow regime models can be substituted in for the models described in this paper. The total pressure drop and void fraction is predicted as the sum of the flow regime time fractions multiplied by the corresponding model for that flow regime. In this way accurate models for the prediction of both pressure drop and void fraction in microchannels are developed, which incorporate flow regime information in a full range of qualities and mass fluxes.

2. Literature review

2.1. Two-phase flow mapping

Garimella [1], Garimella et al. [2], Coleman and Garimella [3], El Hajal et al. [4], Thome et al. [5], Didi et al. [6], Zurcher et al. [7,8], Mandhane et al. [9], and Baker [10] have all described the importance of using flow pattern information in the determination of accurate two-phase flow models. Consequently, much attention has been directed towards developing two-phase flow regime maps. There are three main types of two-phase flow maps in the

* Corresponding author. Tel.: +1 217 377 8249; fax: +1 217 333 1942.
E-mail address: jassim@uiuc.edu (E.W. Jassim).

0017-9310/$ - see front matter © 2006 Elsevier Ltd. All rights reserved.
doi:10.1016/j.ijheatmasstransfer.2006.01.034

Nomenclature

A	cross-sectional area of the microchannel flow
a	curve fit constant
b	curve fit constant
c	curve fit constant
D_h	hydraulic diameter
d	curve fit constant
dP	pressure drop
dz	unit length
F	observed time fraction
f_D	Darcy friction factor
f_{vo}	vapor only friction factor
G	mass flux
g	curve fit constant
KE_{Avg}	average kinetic energy of the flow
P	microchannel wetted perimeter
Re_h	Reynolds number based on the hydraulic diameter
We_v	Weber number for vapor
X_{tt}	Lockhart–Martinelli parameter
X_{ann}	defined by Eq. (12)
x	flow quality

Greek symbols

α	void fraction
ρ	density
$\rho_{2\phi}$	two-phase density
σ	surface tension
μ	dynamic viscosity
Φ^2_{vo}	vapor only two-phase multiplier

Subscripts

l	liquid
liq	pertaining to the liquid flow regime
int	pertaining to the intermittent flow regime
v	vapor
vap	pertaining to the vapor flow regime
ann	pertaining to the annular flow regime

literature: Baker/Mandhane type, Taitel–Dukler type, and Steiner type. Baker [10] developed one of the first two-phase flow regime maps with air–water and air–oil data in large tubes. Baker [10] used superficial vapor mass flux times a fluid property scaling factor on the vertical axes and superficial liquid mass flux times a different fluid property scaling factor on the horizontal axis. Mandhane et al. [9] later developed a similar map with air water data, but used superficial gas and liquid velocities on the horizontal and vertical axes, respectively. Dobson and Chato [11] then made modifications to the flow map of Mandhane et al. [9] by multiplying the axis by the square root of the vapor to air density ratio. Taitel–Dukler [12] developed a mechanistic type flow map with the Lockhart–Martinelli parameter on the horizontal axis and a modified Froude rate times a transition criteria on the vertical axis. Most of the recent two-phase flow regime maps found in the literature are Steiner type flow maps of the form found in Coleman and Garimella [3] as seen in Fig. 1, Garimella [1], Garimella et al. [2], El Hajal et al. [4], Thome et al. [5], and Didi et al. [6] all use similar Steiner style flow maps with quality on the horizontal axis and mass flux on the vertical axis. Some, like Chung and Kawaji [13] use the average flow velocity in the microchannel instead of mass flux on the vertical axis. All three types of flow maps indicate a particular flow regime at any given flow condition with lines dividing the transitions. This seems to lack a physical basis as Coleman and Garimella [3] and El Hajal et al. [4] indicate that more than one flow regime seems to exist near the boundaries. This poses a problem when attempting to develop pressure drop, void fraction, and heat transfer models that incorporate all flow regimes without having discontinuities at the boundaries. In addition, it is very difficult to implement this type of flow map into a model because the flow map cannot readily be represented by continuous functions for all quality ranges. The presence of more than one flow regime at the flow map boundaries seems to indicate that a probabilistic representation of the flow regimes may be better suited in describing the flow.

Niño [14] presented two-phase flow mapping in horizontal microchannels in a distinctly different manner than found in the rest of the literature indicated above. Instead of definitively categorizing the flow regime at a given mass flux and quality, they recorded the time fraction in which each flow regime was observed in each channel at a given mass flux and quality. This was accomplished by obtaining

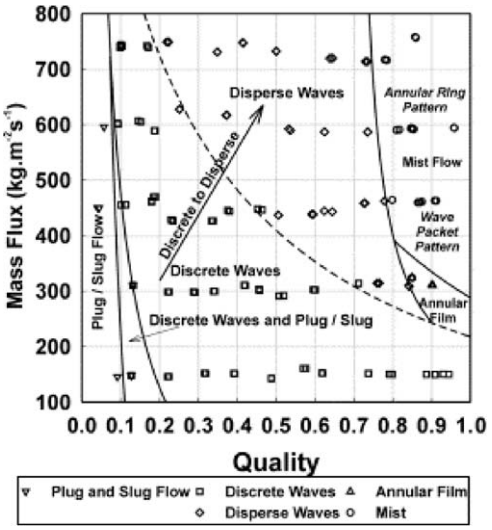

Fig. 1. Typical two-phase flow map from Coleman and Garimella [3].

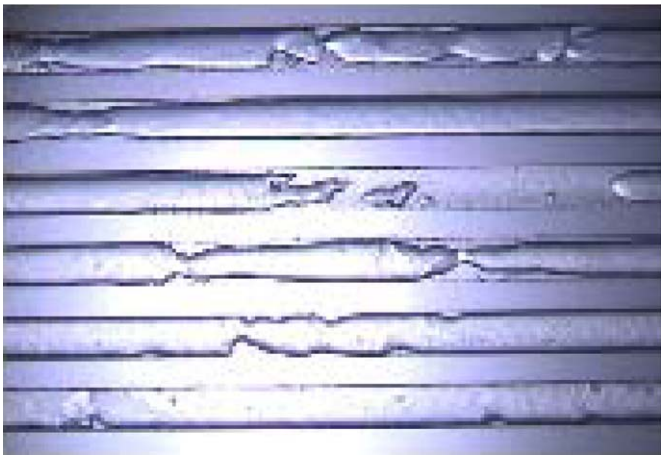

Fig. 2. Picture of R134a at 10 °C flowing through 6-port microchannels (1.54 mm hydraulic diameter) at quality = 17% and mass flux = 100 kg/m^2 s obtained from Niño [14].

numerous pictures of a given mass flux and quality at evenly spaced time intervals. This probabilistic flow mapping technique is especially important for microchannels where each channel may simultaneously exhibit different flow regimes as can be seen in the flow visualization picture in Fig. 2. From Fig. 2 it can be seen that some of the channels are in the annular flow regime and others are seen to be in an intermittent flow regime. Moreover, the flow regime is seen to differ in the same channel at a given flow condition depending on the location of the observation. Figs. 3–14 show probabilistic flow maps with data obtained from Niño [14]. From these figures it can be seen that the total time fraction of all flow regimes present add up to 1. Furthermore, the transitions between flow regimes are smooth. However, no functions were developed for describing the time fraction data nor was the data incorporated in any flow regime models.

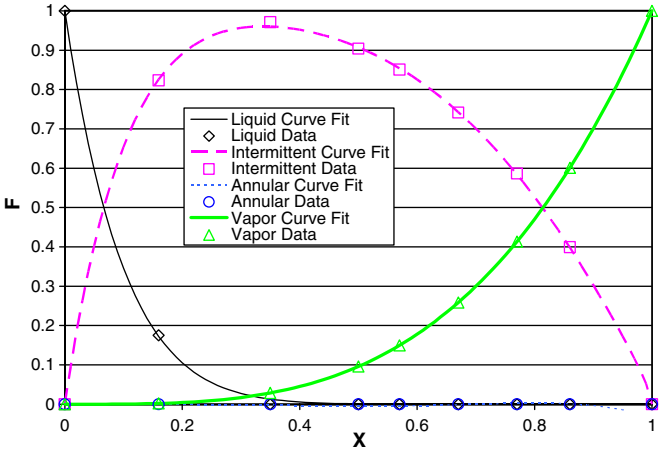

Fig. 3. Probabilistic flow map with time fraction curve fits for R410A at 10 °C and a mass flux of 50 kg/m^2 s in a 6-port microchannel (data obtained from Niño [14]).

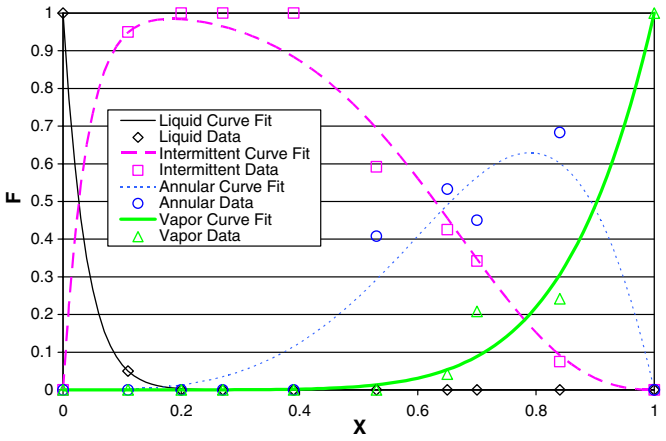

Fig. 4. Probabilistic flow map with time fraction curve fits for R410A at 10 °C and a mass flux of 100 kg/m^2 s in a 6-port microchannel (data obtained from Niño [14]).

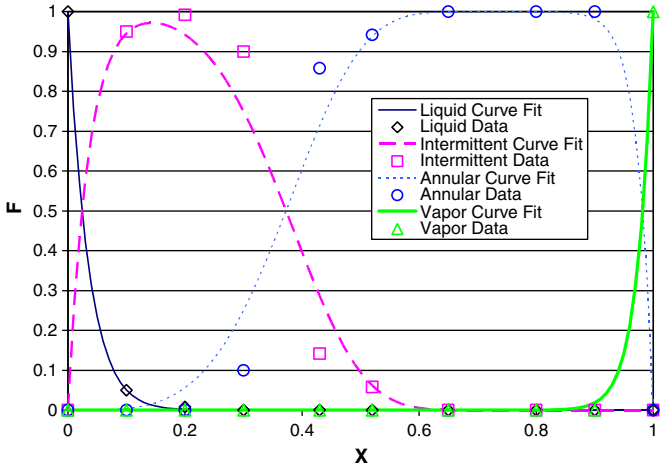

Fig. 5. Probabilistic flow map with time fraction curve fits for R410A at 10 °C and a mass flux of 200 kg/m^2 s in a 6-port microchannel (data obtained from Niño [14]).

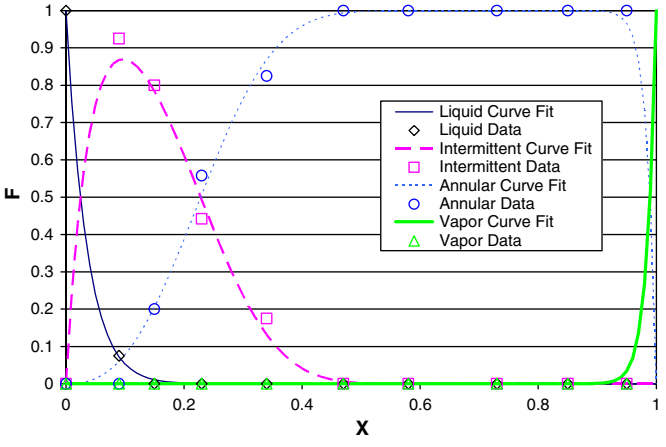

Fig. 6. Probabilistic flow map with time fraction curve fits for R410A at 10 °C and a mass flux of 300 kg/m^2 s in a 6-port microchannel (data obtained from Niño [14]).

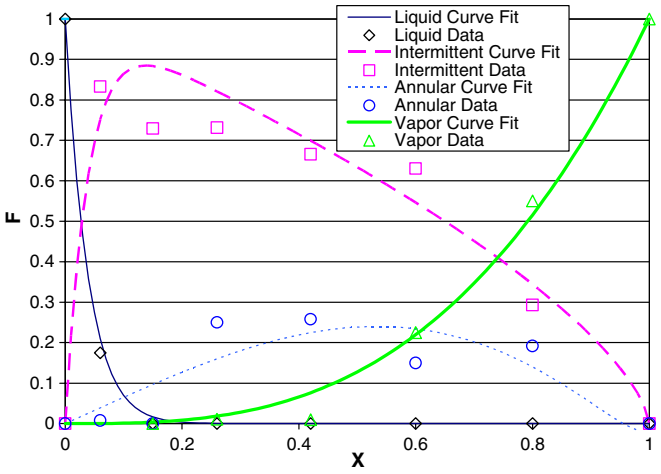

Fig. 7. Probabilistic flow map with time fraction curve fits for R134a at 10 °C and a mass flux of 50 kg/m^2 s in a 6-port microchannel (data obtained from Niño [14]).

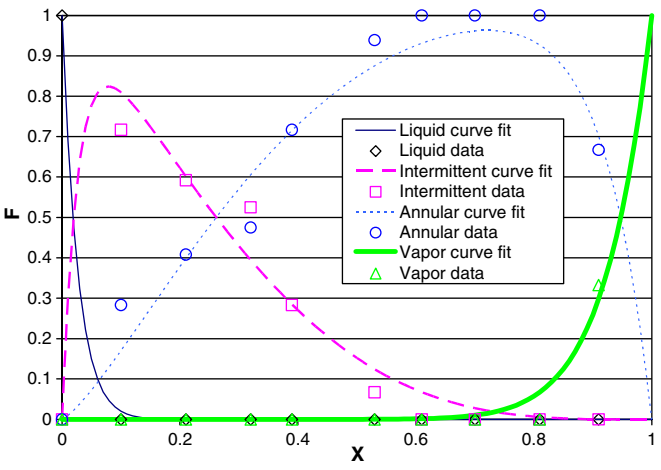

Fig. 8. Probabilistic flow map with time fraction curve fits for R134a at 10 °C and a mass flux of 100 kg/m^2 s in a 6-port microchannel (data obtained from Niño [14]).

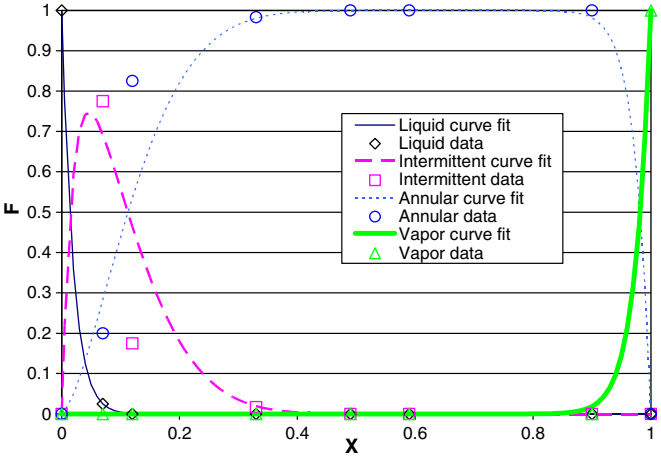

Fig. 9. Probabilistic flow map with time fraction curve fits for R134a at 10 °C and a mass flux of 200 kg/m^2 s in a 6-port microchannel (data obtained from Niño [14]).

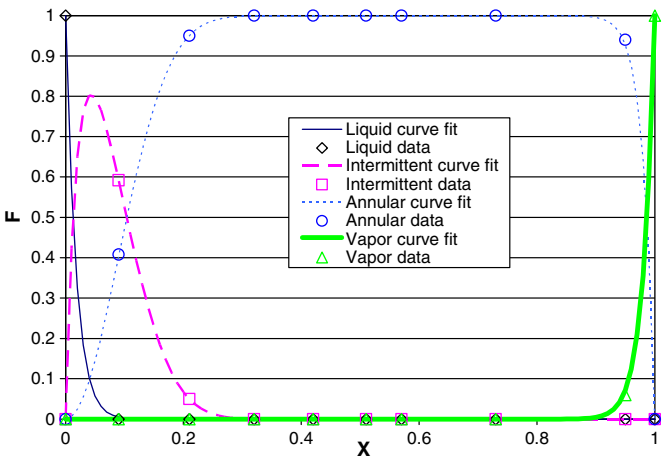

Fig. 10. Probabilistic flow map with time fraction curve fits for R134a at 10 °C and a mass flux of 300 kg/m^2 s in a 6-port microchannel (data obtained from Niño [14]).

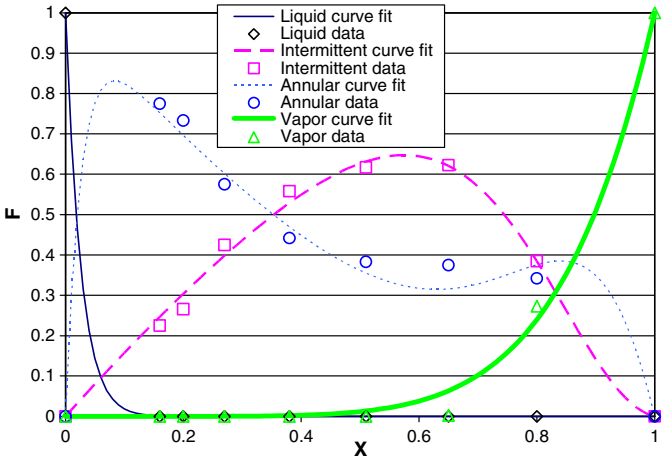

Fig. 11. Probabilistic flow map with time fraction curve fits for air–water at 10 °C and a mass flux of 50 kg/m^2 s in a 6-port microchannel (data obtained from Niño [14]).

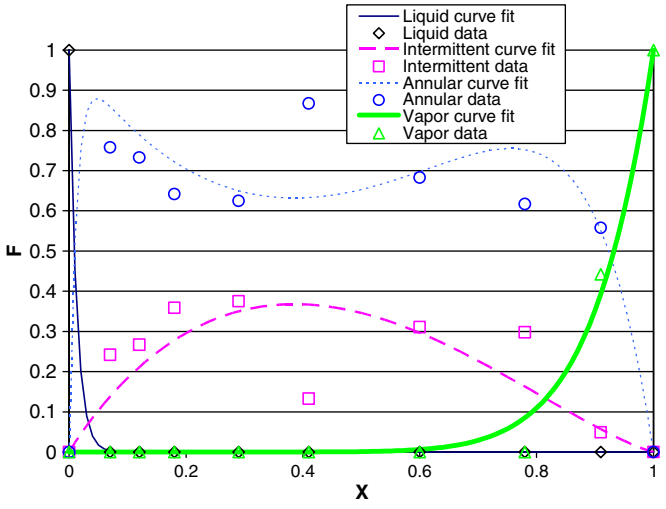

Fig. 12. Probabilistic flow map with time fraction curve fits for air–water at 10 °C and a mass flux of 100 kg/m^2 s in a 6-port microchannel (data obtained from Niño [14]).

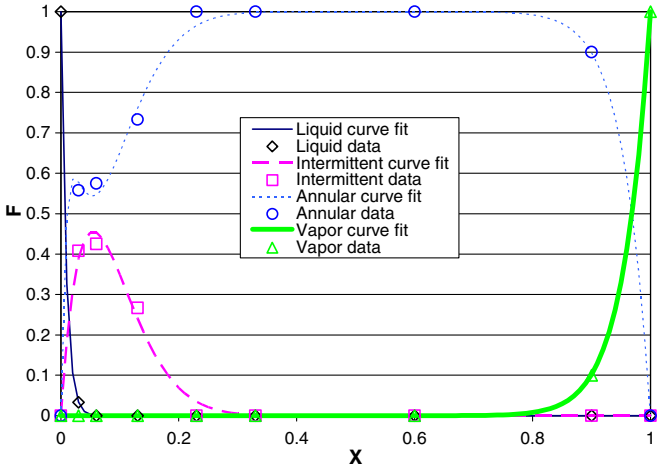

Fig. 13. Probabilistic flow map with time fraction curve fits for air–water at 10 °C and a mass flux of 200 kg/m^2 s in a 6-port microchannel (data obtained from Niño [14]).

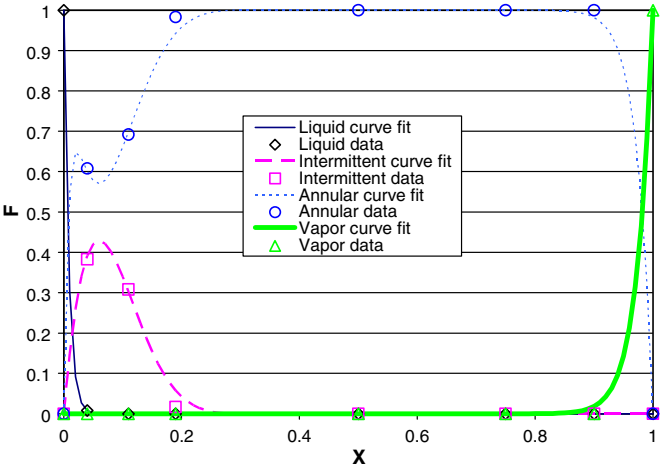

Fig. 14. Probabilistic flow map with time fraction curve fits for air–water at 10 °C and a mass flux of 300 kg/m^2 s in a 6-port microchannel (data obtained from Niño [14]).

2.2. Two-phase pressure drop models

Numerous semi-empirical two-phase pressure drop models have been developed based on assumptions of the nature of the two-phase flow as a whole: homogeneous models and stratified models. Homogeneous flow models assume that the liquid and vapor phases form a homogeneous mixture with the same velocities, whereas the separated flow models assume that the liquid and vapor phases are separate with different velocities. Homogeneous two-phase pressure drop models have been developed for circular tubes such as the one presented by McAdams [15]. Martinelli and Nelson [16], Lockhart and Martinelli [17], Friedel [18], Jung and Radermacher [19], Souza et al. [20], Yang and Webb [21], and Zhang and Kwon [22], Niño [14], and Niño et al. [23] all presented separated flow models which assume two-phase annular flow in tubes. Martinelli and Nelson [16] develop two-phase multipliers to relate the two-phase pressure drop to equivalent flow single-phase pressure drop. Lockhart and Martinelli [17] then correlated the two-phase liquid-only multiplier with the Lockhart–Martinelli parameter, which is the ratio of the frictional pressure drop of the two-phase flow to the frictional pressure drop of the liquid-only flow. However, the Lockhart–Martinelli parameter tends to infinity in an unphysical manner as the quality approaches zero. Friedel [18] utilized the Froude number (ratio of inertial to gravitational forces) and Weber number (ratio of inertial to surface tension forces) to correlate the two-phase liquid only multiplier to round tube data. Jung and Radermacher [19] used the Lockhart–Martinelli parameter in their expression for the two-phase liquid only multiplier in order to correlate their tube refrigerant flow boiling data. Souza et al. [20] utilized both the Lockhart–Martinelli parameter and the Froude number to correlate their data to a two-phase liquid only multiplier. Yang and Webb [21] developed a two-phase pressure drop model, which uses an equivalent single-phase liquid mass flux to correlate R-12 data in microchannels. Zhang and Kwon [22] use a two-phase liquid only multiplier that contains a reduced pressure term in order to correlate refrigerant data in tubes and microchannels. Recently, Niño [14] and Niño et al. [23] (much of the work in Niño et al. [23] is from the thesis Niño [14]) developed a two-phase annular flow pressure drop model for microchannels, which is based on the work of Lockhart and Martinelli [17] and Martinelli and Nelson [16].

Both the homogeneous and separated flow type models are often used in all ranges of qualities and mass fluxes, some of which the assumptions of the physics of the flow do not apply. Recently, some of the literature, such as Didi et al. [6], seek to determine which existing pressure drop model is most accurate for a given flow regime. However, Garimella [1], Garimella et al. [2], and Chung and Kawaji [13] have developed and presented similar flow regime based pressure drop models of the intermittent two-phase flow regime in microchannels, which attempt to incorporate the physics of the flow into the model. These models require the use of a flow regime map to determine the flow regime that exists and require flow visualization data on the slug rate. Flow regime based pressure drop models that incorporate flow visualization information in order to apply the correct physics for full ranges of qualities and mass fluxes were not found in the literature.

2.3. Two-phase void fraction models

Like flow regime based pressure drop modeling, flow regime based modeling of void fraction is in its infancy stage. Numerous semi-empirical two-phase void fraction models have been developed using homogeneous or stratified flow assumptions. The homogeneous two-phase flow void fraction model assumes that the liquid and vapor densities travel at the same velocity. Lockhart and Martinelli [17], Levy [24], Zivi [25], Baroczy [26], Smith [27], Wallis

[28], Premoli et al. [29], Domanski and Didion [30], Ahrens [31], and Bao et al. [32], have all presented void fraction models assuming stratified annular flow in tubes. Kariyasaki et al. [33] and Serizawa et al. [34] found that the void fraction model developed by Armand [35] accurately represents their air–water void fraction data in intermittent flow regime for ~1 mm and ~100 μm channels, respectively. Yashar et al. [36] developed a simple semi-empirical void fraction model that incorporates the Lockhart–Martinelli parameter and the "Froude Rate", a parameter developed by Hurlburt [37]. This model was found to predict void fraction over a large range of conditions. Niño [14] recently developed a semi-empirical two-phase void fraction model assuming annular flow in microchannels, and utilizes the Weber number and Lockhart–Martinelli parameter to correlate the data. Harms et al. [38] developed a mechanistic void fraction model for annular flow in horizontal tubes. However, the above void fraction models are typically used in all ranges of qualities and mass fluxes, some of which the assumptions of the physics of the flow do not apply. Flow regime based void fraction models that incorporate flow visualization information in order to apply the correct physics for full ranges of qualities and mass fluxes were not found in the literature.

3. Curve fitting of flow regime time fractions

Curve fits were made for the flow regime time fraction data found in Niño [14] in order to create user friendly flow regime based pressure drop and void fraction models. The time fraction data in Niño [14] was used only qualitatively and was obtained by taking 20 pictures of horizontal flow through a clear PVC 6-port microchannel test section (120 channel images). Consequently, the time fraction data presented in Niño [14] and used in the present paper represents the classification of over 14,000 images. The uncertainty in the time fraction data was found to be less that 17% and was obtained by comparing the time fraction data with 15 vs. 20 pictures used (90 vs. 120 images). The error in the quality measurements is given to be $\pm 0.003x^{-1.193}$, and the error associated with the mass flux measurements is given as less than ±0.5%.

The proposed liquid time fraction curve fit is given in

$$F_{\text{liq}} = (1-x)^{a} \tag{1}$$

This curve fit contains the physical limits of the liquid time fraction with a time fraction of 1 at a quality of 0 and a time fraction of 0 at a quality of 1.

The proposed intermittent curve fit is given in

$$F_{\text{int}} = (1-x)^{(bx^{c})} - (1-x)^{(d)} \tag{2}$$

Eq. (2) also contains the physical limits of the intermittent time fraction with a time fraction of 0 at a quality of both 0 and 1.

In Niño [14] there are vapor time fractions at unexpectedly low qualities such as $x = 0.1$ for low mass fluxes. This low quality vapor is determined to be intermittent flow in the subsequent analysis.

The proposed high quality vapor curve fit is given in Eq. (3). The low quality vapor is subtracted from the total vapor time fraction observations in order to obtain the high quality vapor time fraction values:

$$F_{\text{vap}} = x^{g} \tag{3}$$

Eq. (3) contains the physical limits of vapor time fraction with a time fraction of zero at a quality of 0 and a time fraction of 1 at a quality of 1.

The proposed annular curve fit is simply one minus the sum of all other flow regime time fractions as seen in Eq. (4). By definition the total time fraction of all flow regimes must be identically equal to 1:

$$F_{\text{ann}} = 1 - F_{\text{liq}} - F_{\text{int}} - F_{\text{vap}} \tag{4}$$

The above time fraction functions were chosen because they are relatively simple yet represent the time fraction data well. Time fraction curve fits are plotted for R410A at 10 °C and a mass fluxes of 50, 100, 200, and 300 kg/m^2 s in Figs. 3–6, respectively, for R134a at 10 °C and a mass fluxes of 50, 100, 200, and 300 kg/m^2 s in Figs. 7–10, respectively, for air–water at 20 °C and a mass fluxes of 50, 100, 200, and 300 kg/m^2 s in Figs. 11–14, respectively, along with the time fraction data found in Niño [14] for 1.54 mm hydraulic diameter 6-port microchannels. From these figures it can be seen that the curve fits reasonably represent the data. The average absolute error associated with the liquid, intermittent, annular, and vapor curve fits are 0.001, 0.0027, 0.007, and 0.031. The annular curve fit in Fig. 3 is seen to dip below zero which does not have a physical basis. This error occurs because the intermittent, liquid, and vapor curve fits are not perfect, while the annular curve fit is defined as one minus the other curve fit constant values. However, the error resulting from this inaccuracy in the calculation of pressure drop and void fraction is found to be negligible (1.7%). The curve fit constants for the above curve fits of R410A, R134a, and air–water are tabulated in Tables 1a–1c, respectively.

Table 1a
Flow regime time fraction curve fit constants for R410A at 10 °C in 6-port microchannels

	$G = 50$ kg/m^2 s	$G = 100$ kg/m^2 s	$G = 200$ kg/m^2 s	$G = 300$ kg/m^2 s
a	10.08	25.77	28.35	27.87
b	0.66	1.88	23.86	47.32
c	2.24	2.15	2.81	1.98
d	10.08	25.77	28.35	27.87
g	3.38	6.80	37.92	65.58

Table 1b
Flow regime time fraction curve fit constants for R134a at 10 °C in 6-port microchannels

	$G = 50$ kg/m^2 s	$G = 100$ kg/m^2 s	$G = 200$ kg/m^2 s	$G = 300$ kg/m^2 s
a	25.23	36.99	50.92	55.68
b	0.66	3.27	31.82	60.17
c	0.01	0.27	0.62	1.00
d	25.23	36.99	50.92	55.68
g	2.97	12.81	37.75	51.21

Table 1c
Flow regime time fraction curve fit constants for air–water at 20 °C in 6-port microchannels

	$G = 50$ kg/m^2 s	$G = 100$ kg/m^2 s	$G = 200$ kg/m^2 s	$G = 300$ kg/m^2 s
a	30.60	71.09	111 .02	118.28
b	1.20	1.21	29.17	54.34
c	4.04	0.19	0.57	0.93
d	1.62	2.90	22.81	16.86
g	6.40	9.91	21.67	37.94

4. Probabilistic pressure drop modeling

With the time fraction curve fit functions and curve fit constants established, a probabilistic flow regime pressure drop model can be developed for practical use. Pressure drop can be predicted by simply summing the time fraction of a flow regime multiplied by a pressure drop model for the respective flow regime as shown in

$$\left(\frac{dP}{dz}\right)_{total} = F_{liq}\left(\frac{dP}{dz}\right)_{liq} + F_{int}\left(\frac{dP}{dz}\right)_{int} + F_{vap}\left(\frac{dP}{dz}\right)_{vap} + F_{ann}\left(\frac{dP}{dz}\right)_{ann} \quad (5)$$

Consequently, this model applies the appropriate assumptions for a full range of flow conditions. The pressure drop models used for each flow regime are the models that were found by Niño [14] to accurately represent their data for the same channel geometry as used in their flow visualization experiments. Niño [14] does not use the time fraction data in any quantitative manner. Niño et al. [23] present the pressure drop correlations in Niño [14] but do not use the time fraction information in any manner. Eq. (5) allows for the use of different flow regime specific models as more accurate models are identified. The Reynolds number for the microchannels is defined according to Niño [14] work as shown in

$$Re_h = \frac{GD_h}{\mu}, \quad \text{where } D_h = \frac{4A}{P} \quad (6)$$

4.1. Liquid flow pressure drop model

By solving the Navier–Stokes equation the Darcy friction factor used for single phase flow in the laminar regime, $Re_h < 2300$ is given in

$$f_D = \frac{64}{Re_h} \quad (7)$$

The Darcy friction factor used for turbulent flow, $Re_h > 2300$, is given by (Blausius Equation)

$$f_D = \frac{0.3164}{Re_h^{0.25}} \quad (8)$$

The liquid pressure drop is then determined using

$$\frac{dP}{dz} = f_D\left(\frac{1}{D_h}\right)\frac{G^2}{2\rho} \quad (9)$$

Niño [14] found that these relations accurately represent the single-phase pressure drop data that he obtained for microchannels.

4.2. Vapor flow pressure drop model

The vapor pressure drop model is exactly the same as the model used for liquid flow (Eqs. (7)–(9)) since vapor flow is also a single-phase flow.

4.3. Intermittent flow pressure drop model

The intermittent flow pressure drop model developed in Niño [14] is given in Eq. (10) below. This model assumes a homogeneous density and uses the two-phase mixture's average kinetic energy to predict pressure drop.

$$\left(\frac{\Delta P}{\Delta z}\right)_{int} = 0.045\frac{1}{D_h}KE_{Avg}, \quad \text{where } KE_{Avg} = \frac{G^2}{2\rho_{2\phi}} \quad \text{and } \rho_{2\phi} = \left[\frac{x}{\rho_v} + \frac{(1-x)}{\rho_l}\right]^{-1} \quad (10)$$

Niño [14] and Niño et al. [23] found that Eq. (10) accurately predicts their data for intermittent flow pressure drop in microchannels for air–water, R410A, and R134a. Adams [39] found Eq. (10) to be valid for R245fa, carbon dioxide, and ammonia in microchannels when compared to his data.

4.4. Annular flow (separated flow) pressure drop model

The annular flow pressure drop model used, developed in Niño [14] and Niño et al. [23], is given by the following relationship:

$$\left(\frac{dP}{dz}\right)_{2\phi} = \Phi_{vo}^2 \left(\frac{dP}{dz}\right)_{vo} \tag{11}$$

where Φ_{vo}^2 is an experimentally determined two-phase multiplier given by (obtained from Niño et al. [23])

$$\Phi_{vo}^2 = \exp(-0.046X_{ann}) + 0.22[\exp(-0.002X_{ann}) - \exp(-7X_{ann})] \tag{12}$$

where $X_{ann} = \left[\left(X_{tt} + \frac{1}{We_v^{1.3}}\right)\left(\frac{\rho_l}{\rho_v}\right)^{0.9}\right]$, $We_v = \frac{\left[\frac{(xG)^2}{\rho_v}\right]}{\frac{\sigma}{D_h}}$, and

$$X_{tt} = \left(\frac{1-x}{x}\right)^{0.875}\left(\frac{\rho_v}{\rho_l}\right)^{0.5}\left(\frac{\mu_l}{\mu_v}\right)^{0.125}$$

Furthermore, the vapor only pressure drop is determined by the equation below:

$$\left(\frac{dP}{dz}\right)_{vo} = 2f_{vo}\frac{1}{D_h}\frac{G^2}{\rho_v} \tag{13}$$

4.5. Treatment of low quality vapor

The existence of low quality vapor at qualities of 0.3 and less in Niño [14] is unexpected. Vapor flow is normally associated with high quality flow. It is hypothesized, that the flow classified as low quality vapor in the work of Niño [14] may actually be intermittent flow with very long bubbles that are longer than the field of view of the camera. In order to test this hypothesis, the pressure drop model given in Eq. (5) was implemented twice: first treating low quality vapor as vapor, and second treating the low quality vapor as intermittent flow. Treatment of low quality vapor as vapor predicted a significantly higher pressure drop than experimentally obtained at low quality ranges. However, when the low quality vapor was treated as intermittent flow the model was found to represent the data very well. This leads one to believe that the low quality vapor observations found in the work of Niño [14] are in fact intermittent flow. Consequently, the low quality vapor time fraction functions are assumed to be intermittent flow time fractions in the analysis.

4.6. Evaluation of the probabilistic pressure drop model

Using Eq. (5), along with curve fit equations (1)–(4) and pressure drop model Eqs. (6)–(13), pressure drop is predicted for R410A, R134a, and air–water for a range of mass fluxes and qualities. The predicted pressure drop determined by the probabilistic model and the measured pressure drop is plotted for R410A, and R134a at 10 °C with a range of mass fluxes and qualities in Figs. 15 and 16, respectively. The experimental pressure drop data was

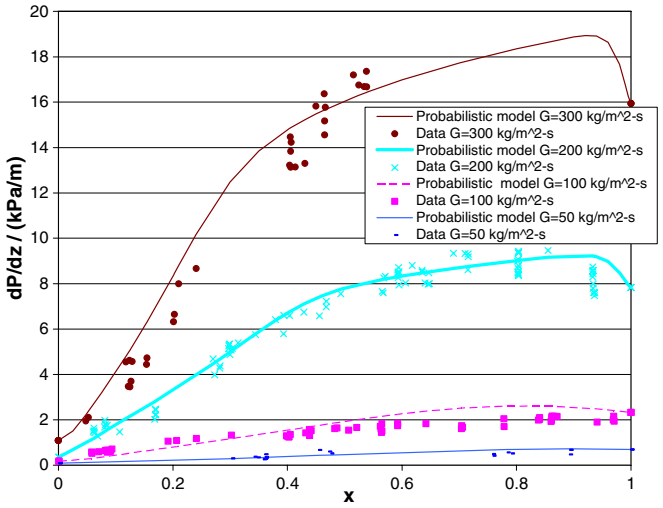

Fig. 15. Predicted and measured pressure drop vs. quality for R410A at 10 °C in 6-port microchannels.

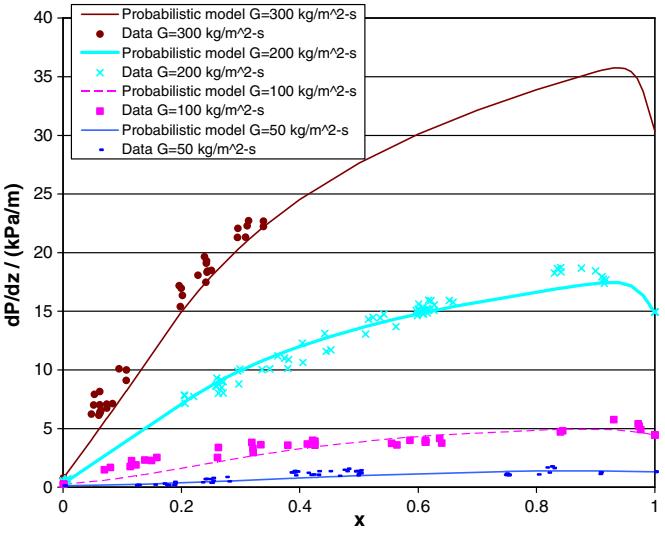

Fig. 16. Predicted and measured pressure drop vs. quality for R134a at 10 °C in 6-port microchannels.

obtained from Niño [14] and was subsequently used in Niño et al. [23]. The reported error associated with these pressure drop measurements is ±0.25%. The pressure drop, and flow visualization time fraction data was obtained by Niño [14] in independent tests. Additional details on the experimental setup and procedures used to obtain this data can be obtained from Niño et al. [23]. From Figs. 15 and 16 it can be seen that the data lies very close to the model lines for all mass fluxes and qualities investigated. Furthermore, it can be seen that the probabilistic model has the correct limits. The predicted pressure drop determined by the probabilistic model and the pressure drop data obtained from Niño [14] is plotted for air–water at 20 °C for a range of mass fluxes and qualities in Fig. 17. The mass fluxes of the pressure drop data found for air–water in Niño [14] were less than 10% higher than the mass fluxes of the probabilistic flow maps that were created. Consequently, it is

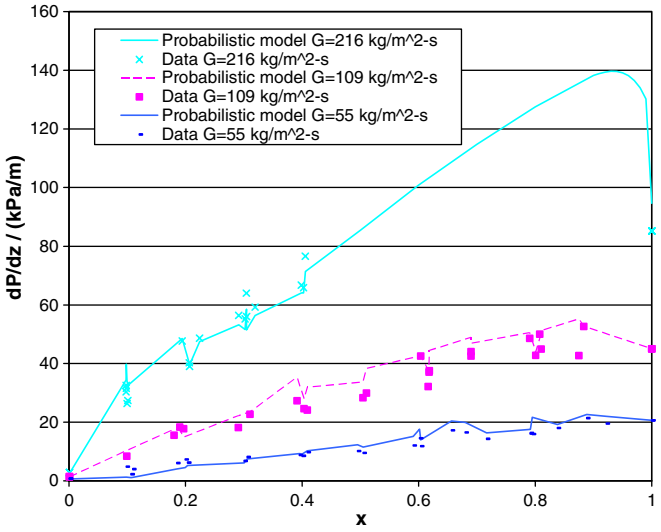

Fig. 17. Predicted and measured pressure drop vs. quality for air–water at 20 °C in 6-port microchannels.

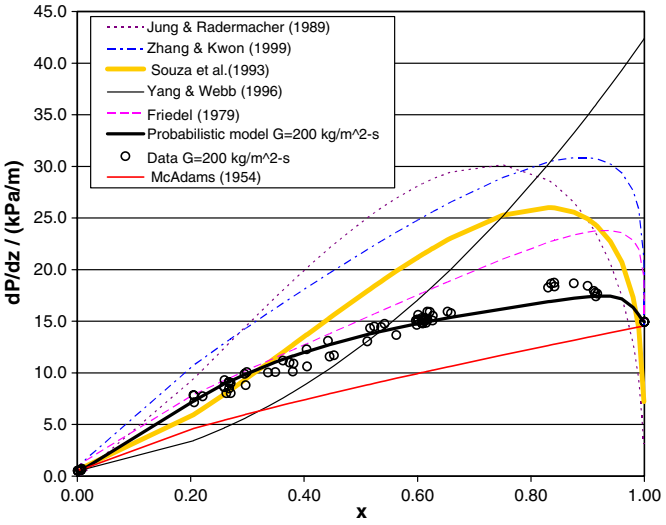

Fig. 18. Comparison of pressure drop models for R134a at 10 °C and $G = 200$ kg/m^2 s in 6-port microchannels.

reasonable to compare the data to the probabilistic model. From Fig. 17 it can be seen that the pressure drop data lie very close to the probabilistic model line. The probabilistic model curves are not smooth due to differences in the air supply pressure for the various flow conditions. The air pressure variations resulted in different vapor densities from point to point, so the probabilistic model pressure drop was determined for each point using the actual vapor density found at that data point. A constant vapor density was assumed in the high quality regions where the experimental data were not available in order to show the high quality range trends. The problem associated with varying vapor densities does not exist with the refrigerant data because the vapor density is a function of the saturation temperature. In the air–water experiments the vapor density is almost entirely a function of the air pressure and temperature supplied because the partial pressure of the water vapor is minimal.

In order to further illustrate the accuracy of the probabilistic flow map model it is compared with the pressure drop data found in Niño [14] for 6-port microchannels and with several other pressure drop models in Fig. 18. From this figure it can be seen that the probabilistic flow map model best represents the data for most quality ranges as it is seen to have essentially the same trends as the data with physically correct limits as the quality approaches zero or one. The Jung and Radermacher [19], and Sousa et al. [20] models approach zero as the quality approaches 1, which lack physical significance because they both contain a $(1 - x)$ term in the numerator of their two-phase multiplier expressions. The Yang and Webb [21] model also lacks a physically correct pressure drop, because the pressure drop is much higher than vapor only pressure drop as the quality approaches 1. The probabilistic model pressure drop predictions vs. the measured pressure drop values are plotted in Fig. 19 for R410A, R134a, and

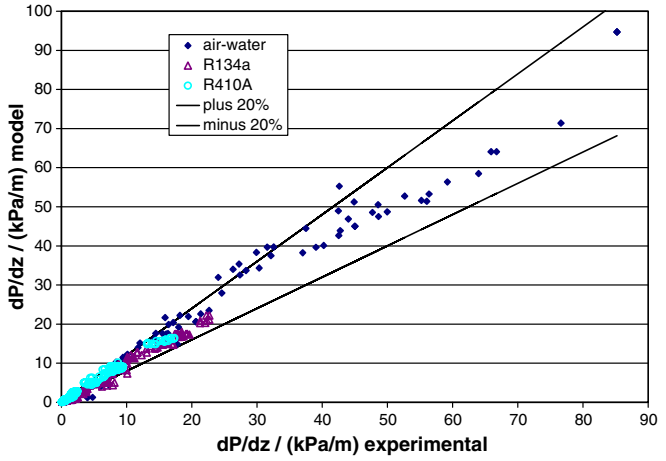

Fig. 19. Model vs. experimental pressure drop for air–water, R134a, and R410a in 6-port microchannels.

air–water. From Fig. 19 it can be seen that the model error mostly lies within 20% error lines. The percentage of predicted values that lie within 20% error lines are tabulated in Table 2 in order to further compare the accuracy of the probabilistic model with the correlations found in Fig. 18. It is evident from Table 2 that the probabilistic model performs better that the rest of the models except for air–water pressure drop with the McAdams [15] model performing equally well.

5. Probabilistic void fraction modeling

Probabilistic flow regime map based modeling can be applied to void fraction as well. Similar to pressure drop, void fraction can be modeled by simply summing the time fraction of a flow regime multiplied by a void fraction

Table 2
Percentage of two-phase pressure drop predictions that lie within a 20% error band for different models based upon Niño [14] data (chart is modified from Niño [14])

Pressure drop model	R410A	R134a	Air–water
Probabilistic model	66%	70%	76%
McAdams [15]	45%	25%	76%
Friedel [18]	48%	25%	22%
Jung and Radermacher [19]	18%	17%	0%
Souza et al. [20]	41%	8%	0%
Yang and Webb [21]	25%	21%	13%
Zhang and Kwon [22]	36%	27%	11%

model for the respective flow regime as shown in the equation below:

$$\alpha_{total} = F_{liq}\alpha_{liq} + F_{int}\alpha_{int} + F_{vap}\alpha_{vap} + F_{ann}\alpha_{ann} \quad (14)$$

Many of the models used for the individual flow regimes were obtained from Niño [14] where he found them to represent his void fraction data well for the same channel geometry as used in his flow visualization experiments. However, other flow regime specific void fraction models could be used as more accurate models are identified. Niño [14] does not use the time fraction data in his void fraction models in any quantitative manner.

5.1. Liquid and vapor void fraction model

By definition, the liquid only flow void fraction is identically equal to 0, and the vapor only flow void fraction is identically equal to 1.

5.2. Intermittent flow void fraction

The Armand [35] void fraction model, Eq. (15), is utilized for the intermittent flow void fraction model component because of its simplicity and good predictive capabilities as seen in the literature:

$$\alpha_{int} = \frac{(0.833 + 0.167x)x\left(\frac{1}{\rho_v}\right)}{(1-x)\left(\frac{1}{\rho_l}\right) + x\left(\frac{1}{\rho_v}\right)} \quad (15)$$

5.3. Annular flow void fraction

The annular flow void fraction model used in the probabilistic model utilizes the Weber number and the Lockhart Martinelli parameter, just as modeled in the pressure drop model for annular flow. The equation for the annular flow void fraction model, developed by Niño [14], is given below:

$$\alpha_{ann} = \left[1 + \left(X_{tt} + \frac{1}{We_v^{1.3}}\right)\left(\frac{\rho_l}{\rho_v}\right)^{0.9}\right]^{-0.06} \quad (16)$$

where X_{tt}, and We_v are defined in Eq. (12) above.

5.4. Evaluation of the probabilistic void fraction model

Using Eq. (14), along with curve fit equations (1)–(4) and void fraction model Eqs. (15) and (16), void fraction is predicted for R410A, R134a, and air–water for a range of mass fluxes and qualities. The probabilistic void fraction model and void fraction data are plotted for R410A and R134a at 10 °C for a range of mass fluxes and qualities in Figs. 20 and 21, respectively. In addition, the probabilistic void fraction model and void fraction data are plotted for air–water at 20 °C in Fig. 22. The void fraction data was obtained from Niño [14]. Niño [14] obtained the void fraction data by pneumatically crimping the ends of an aluminum microchannel sections and comparing the weight of the empty and full sections. The reported error in the void

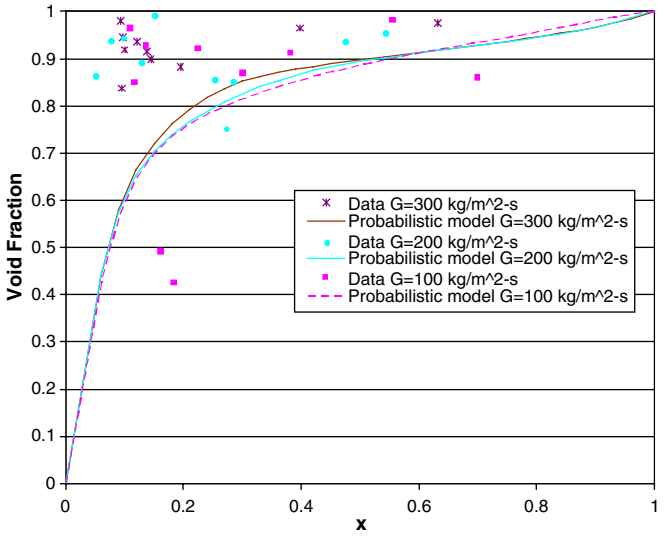

Fig. 20. Predicted and measured void fraction vs. quality for R410A at 10 °C in 6-port microchannels.

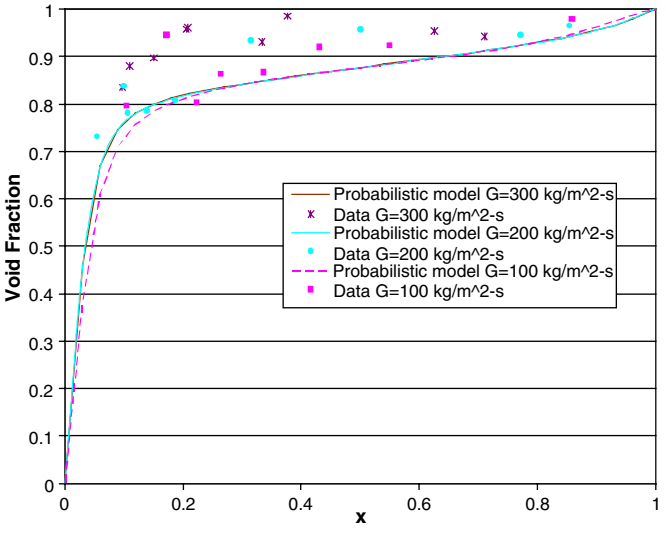

Fig. 21. Predicted and measured void fraction vs. quality for R134a at 10 °C in 6-port microchannels.

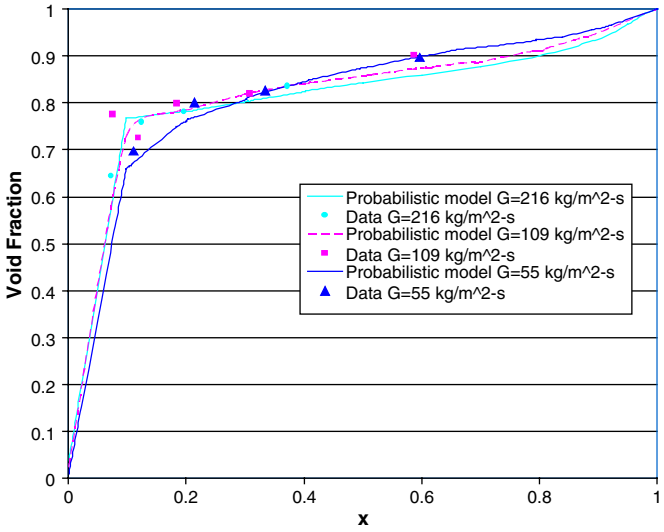

Fig. 22. Predicted and measured void fraction vs. quality for air–water at 20 °C in 6-port microchannels.

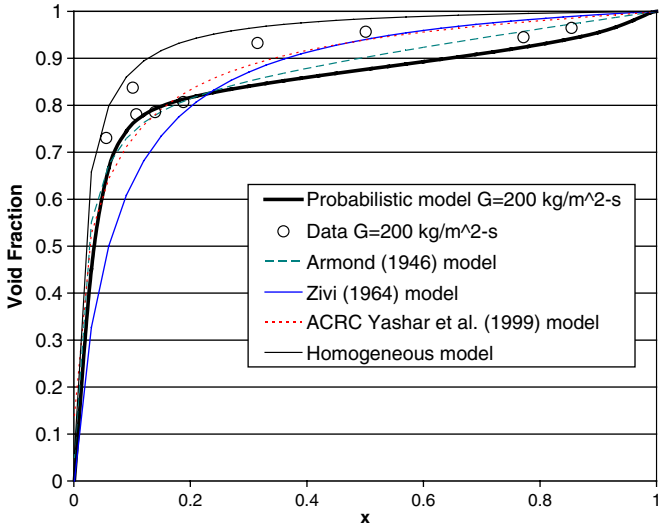

Fig. 23. Comparison of void fraction models for R134a at 10 °C and $G = 200\ \mathrm{kg/m^2\,s}$ in 6-port microchannels.

fraction measurements is less than ±0.7% if the test section is sealed perfectly. The error in the quality measurements is given to be $\pm 0.003x^{-1.193}$.

From Figs. 20 to 22 it can be seen that the data lies close to the probabilistic model curves for the range of qualities and mass fluxes investigated. The deviation from the model can partly be attributed to the fact that the crimping process is not perfect which can lead to a large error associated with the void fraction measurements. The R410A, high pressure refrigerant, data is found to have the most scatter and the air–water data (lowest pressure) is found to have the least scatter. This seems to indicate that the test sections were leaking. Fig. 23 compares the probabilistic flow regime map based void fraction model with other models.

6. Conclusion

Many pressure drop and void fraction models can be found in the literature, however the assumptions which they use tend to only apply to a particular flow regime. Probabilistic two-phase flow regime maps are found to be suitable flow maps for incorporating flow regime information into pressure drop and void fraction models. Curve fits were developed for liquid, intermittent, annular, and vapor flow regime time fractions for R410A, R134a, and air–water probabilistic flow regime maps for 6-port microchannels. These curve fit functions capture the time fraction physical limits. Probabilistic pressure drop and void fraction models based on the time fraction curve fits of the two-phase flow were developed. This method is unique in that the flow is modeled based on the actual physical flow field characteristics, which allows the incorporation of the appropriate weighting of the respective two-phase flow models. It was found that the probabilistic flow regime map based pressure drop model predicts pressure drop very well. Moreover, the probabilistic flow mapping based void fraction model predicts void fraction close to the data. However, more accurate void fraction data must be obtained in order to further evaluate the probabilistic flow mapping based void fraction model. Consequently, the probabilistic flow mapping based modeling technique has the potential to be a useful tool in predicting pressure drop and void fraction in microchannels. Caution should be exercised in using the models developed for other geometries and conditions outside of the ones in which the probabilistic flow maps were developed. In the future we hope to link the curve fit constants to physical parameters such as mass flux, hydraulic diameter, and vapor density in order to obtain a model that is more generally applicable.

Acknowledgement

The authors would like to thank the Air Conditioning and Research Center (ACRC) at the University of Illinois for their financial support.

References

[1] S. Garimella, Condensation flow mechanisms in microchannels: basis for pressure drop and heat transfer models, Heat Transfer Eng. 25 (3) (2004) 104–116.
[2] S. Garimella, J.D. Killion, J.W. Coleman, An experimentally validated model for two-phase pressure drop in the intermittent flow regime for noncircular microchannels, J. Fluids Eng. 125 (2003) 887–894.
[3] J.W. Coleman, S. Garimella, Two-phase flow regimes in round, square and rectangular tubes during condensation of refrigerant R134a, Int. J. Refrig. 26 (2003) 117–128.
[4] J. El Hajal, J.R. Thome, A. Cavalini, Condensation in horizontal tubes, part 1: two-phase flow pattern map, Int. J. Heat Mass Transfer 46 (2003) 3349–3363.
[5] J.R. Thome, J. El Hajal, A. Cavalini, Condensation in horizontal tubes, part 2: new heat transfer model based on flow regimes, Int. J. Heat Mass Transfer 46 (2003) 3365–3387.

[6] M.B. Didi, N. Kattan, J.R. Thome, Prediction of two-phase pressure gradients of refrigerants in horizontal tubes, Int. J. Refrig. 25 (2002) 935–947.
[7] O. Zurcher, D. Farvat, J.R. Thome, Development of a diabetic two-phase flow pattern map for horizontal flow boiling, Int. J. Heat Mass Transfer 45 (2002) 291–301.
[8] O. Zurcher, D. Farvat, J.R. Thome, Evaporation of refrigerants in a horizontal tube: and improved flow pattern dependent heat transfer model compared to ammonia data, Int. J. Heat Mass Transfer 45 (2002) 303–317.
[9] J.M. Mandhane, G.A. Gregory, K. Aziz, A flow pattern map for gas–liquid flow in horizontal and inclined pipes, Int. J. Multiphase Flow 1 (1974) 537–553.
[10] O. Baker, Simultaneous flow of oil and gas, Oil Gas J. 53 (1954) 185–195.
[11] M.K. Dobson, J.C. Chato, Condensation in smooth horizontal tubes, J. Heat Transfer 120 (1998) 192–213.
[12] Y. Taitel, A.E. Dukler, A model for predicting flow regime transitions in horizontal and near horizontal gas–liquid flow, Am. Inst. Chem. Eng. J. 22 (1976) 47–55.
[13] P.M.-Y. Chung, M. Kawaji, The effect of channel diameter on adiabatic two-phase flow characteristics in microchannels, Int. J. Multiphase Flow 30 (2004) 735–761.
[14] V.G. Niño, Characterization of two-phase flow in microchannels, Ph.D. Thesis, University of Illinois, Urbana-Champaign, IL, 2002.
[15] W.H. McAdams, Heat Transmission, third ed., McGraw Hill, New York, 1954.
[16] R.C. Martinelli, B. Nelson, Prediction of pressure drop during forced-circulation boiling water, Trans. ASME 70 (1948) 695–702.
[17] R.W. Lockhart, R.C. Martinelli, Proposed correlation of data for isothermal two-phase, two-component flow in pipes, Chem. Eng. Progr. 45 (Part 1) (1949) 39–48.
[18] L. Friedel, Improved friction pressure drop correlations for horizontal and vertical two phase pipe flow, in: European Two-Phase Flow Group Meeting, Ispra, Italy, 1979, Paper E2.
[19] D.S. Jung, R. Radermacher, Prediction of pressure drop during horizontal annular flow boiling of pure and mixed refrigerants, Int. J. Heat Mass Transfer 32 (12) (1989) 2435–2446.
[20] A.L. Souza, J.C. Chato, J.P. Wattelet, B.R. Christoffersen, Pressure drop during two-phase flow of pure refrigerants and refrigerant-oil mixtures in horizontal smooth tubes, Heat Transfer Alter. Refrig. (ASME) HTD 243 (1993) 35–41.
[21] C.Y. Yang, R.L. Webb, Friction pressure drop of R12 in small hydraulic diameter extruded aluminum tubes with and without micro-fins, Int. J. Heat Mass Transfer 39 (4) (1996) 801–809.
[22] M. Zhang, S.L. Kwon, Two-phase frictional pressure drop for refrigerants in small diameter tubes, in: R.K. Shah (Ed.), Compact Heat Exchangers and Enhancement Technology for the Process Industries, Begell House, New York, 1999.
[23] V.G. Niño, E.W. Jassim, P.S. Hrnjak, T.A. Newell, Flow-regime based model for pressure drop predictions in microchannels, HVAC&R Res. 12 (1) (2006) 17–34.
[24] S. Levy, Steam slip theoretical prediction from momentum model, Trans. ASME, J. Heat Transfer C 82 (1960) 113–124.
[25] S.M. Zivi, Estimation of steady-state steam void fraction by means of the principle of minimum entropy production, Trans. ASME, J. Heat Transfer C 86 (1964) 247–252.
[26] C.J. Baroczy, Correlation of liquid fraction in two-phase flow with application to liquid metals, Chem. Eng. Progr. Sympos. Ser. 61 (57) (1965) 179–191.
[27] S.L. Smith, Void fractions in two-phase flow: a correlation based upon an equal velocity head model, Proc. Instn. Mech. Engrs., Lond. 184 (36) (1969) 647–664.
[28] G.B. Wallis, One Dimensional Two-Phase Flow, McGraw Hill, New York, 1969, pp. 51–54.
[29] A. Premoli, D. Francesco, A. Prina, A dimensional correlation for evaluating two-phase mixture density, La Termotecnica 25 (1) (1971) 17–26.
[30] P. Domanski, D. Didion, Computer modeling of the vapor compression cycle with constant flow area expansion device, NBS-BSS-155, Springfield, VA, 1983, pp. 1–163.
[31] F.W. Ahrens, Heat pump modeling, simulation, and design: heat pump fundamentals, in: Proceedings of the NATO Advanced Study Institute on Heat Pump Fundamentals, Martinus Nijhoff Publishers, Espinho, 1980, pp. 155–191.
[32] Z.Y. Bao, M.G. Bosnish, B.S. Haynes, Estimation of void fraction and pressure drop for two-phase flow in fine passages, Trans. Inst. Chem. Eng. A 72 (1994) 625–632.
[33] A. Kariyasaki, T. Fukano, A. Ousaka, M. Kagawa, Characteristics of time-varying void fraction in isothermal air–water cocurrent flow in horizontal capillary tube, Trans. JSME 57 (544) (1991) 4036–4043.
[34] A. Serizawa, Z. Feng, Z. Kawara, Two phase flow in microchannels, Exp. Thermal Fluid Sci. 26 (6–7) (2002) 703–714.
[35] A.A. Armand, The resistance during the movement of a two-phase system in horizontal pipes, Izv. Vses. Teplotekh. Inst. 1 (1946) 16–23.
[36] D.A. Yashar, M.J. Wilson, H.R. Kopke, D.M. Graham, J.C. Chato, T.A. Newell, An investigation of refrigerant void fraction in horizontal, microfin tubes, ACRC report TR-145, University of Illinois at Urbana-Champaign, 1999.
[37] E.T. Hurlburt, Modeling of the evaporation and condensation of zeotropic refrigerants mixtures in horizontal, annular flow, Ph.D. Thesis, University of Illinois, Urbana-Champaign, IL, 1997.
[38] T.M. Harms, D. Li, A.E. Groll, J.E. Braun, A void fraction model for annular flow in horizontal tubes, Int. J. Heat Mass Transfer 46 (2003) 4051–4057.
[39] D. Adams, Pressure drop and void fraction in microchannels using carbon dioxide, ammonia and R245fa as refrigerants, M.S. Thesis, University of Illinois, Urbana-Champaign, IL, 2003.